forests

MDPI

Article

Assessing Forest Habitat Structure with LiDAR Across Ungulate Management Gradients

Claudia C. Jordan-Fragstein [1,*], Katharina Gungl [2], Dominik Seidel [3] and Michael G. Müller [1]

[1] Chair of Forest Protection, Technische Universität Dresden, 01737 Tharandt, Germany; michael.mueller@tu-dresden.de
[2] Staatsbetrieb Sachsenforst, Bonnewitzer Straße 34, 01796 Pirna, Germany; katharina.gungl@smekul.sachsen.de
[3] Department for Spatial Structures and Digitization of Forests, Georg-August-Universität Göttingen, 37077 Göttingen, Germany; dseidel@gwdg.de
* Correspondence: claudia.jordan-fragstein@tu-dresden.de; Tel.: +49-4015155624424

Abstract

Ungulate browsing is a major driver of forest regeneration dynamics and habitat structure in managed temperate forests, influencing species composition, regeneration success, and long-term stand development. Traditional assessments of browsing impacts often rely on field-based indicators such as regeneration density or visual cover, but these metrics provide limited insight into three-dimensional habitat structure. Mobile handheld LiDAR offers highly detailed measurements of forest structure, enabling objective and reproducible quantification of structural complexity that complements and extends conventional field-based methods. In this study, we applied handheld LiDAR as an innovative indicator for habitat structure within the ungulate browsing zone (<2 m height) to evaluate structural development across sites differing in management context. Paired fenced and unfenced plots (12 × 12 m) were surveyed within the WiWaldI project framework in 2019 and 2023 and compared across three hunting regimes representing different degrees of ungulate population management. Structural complexity was quantified by deriving box-counting dimensions from LiDAR point clouds, providing a measure of spatial arrangement and density relevant to ungulate–vegetation interactions. To support interpretation and ecological context, we complemented LiDAR indicators with streamlined field assessments. Based on this framework, we assessed whether forest structural complexity and visual cover differ among regions and over time, and whether ungulate browsing induces detectable structural differences between fenced whether structural differences between fenced and unfenced plots are detectable. We further examined the relative importance of tree species composition, plant architecture, and hunting regime as drivers of three-dimensional habitat structure. A simplified octant method characterized the spatial distribution of woody regeneration, while a silhouette-based approach quantified visual cover from the perspective of a standard ungulate profile. These auxiliary measures contextualize visual and spatial aspects of structure that LiDAR metrics capture with minimal observer bias. LiDAR studies have previously demonstrated potential for linking high-resolution structural data to ungulate habitat use, and our approach extends this by focusing on structural complexity as a habitat indicator. Results show a consistent increase in LiDAR-derived structural complexity between 2019 and 2023 across all regions. This increase occurred across management contexts and was not consistently explained by fencing or hunting regime effects, suggesting that site conditions, forest composition, and successional processes were dominant drivers during the observation period. Hunting regime showed no statistically significant and no consistent effect on structural complexity across regions or years. Visual cover metrics varied strongly among regions and species and declined over time. These findings suggest that

Check for updates

Academic Editor: Shengbin Chen

Received: 22 January 2026
Revised: 18 February 2026
Accepted: 24 February 2026
Published: 26 February 2026

Copyright: © 2026 by the authors. Licensee MDPI, Basel, Switzerland. This article is an open access article distributed under the terms and conditions of the Creative Commons Attribution (CC BY) license.

three-dimensional habitat structure information has the potential to enhance the evaluation of ungulate impacts and may support evidence-based forest and wildlife management, particularly when interpreted in the context of site conditions and successional dynamics. Beyond ungulate impact assessment, the presented handheld LiDAR approach provides a scalable remote sensing framework for precision forestry by capturing three-dimensional structural attributes that are directly linked to forest stability, resilience, growth dynamics, and stand-level species mixing, thereby supporting evidence-based forest management recommendations.

Keywords: ungulate management; forest regeneration; habitat structure; structural complexity; LiDAR; box-counting dimension; mixed forests; browsing; ungulates; forest management

1. Introduction

Ungulate browsing represents a major ecological driver in temperate forest ecosystems, influencing regeneration dynamics, tree species composition, and structural development [1–5]. Selective browsing alters competitive relationships among saplings and can shift successional trajectories, particularly where browsing pressure exceeds tolerance thresholds of regenerating tree species [2,3]. These impacts extend beyond species composition to structural attributes of forest stands, affecting vertical layering, stem density, and spatial heterogeneity within the browsing-relevant height layer. Consequently, understanding how browsing interacts with site conditions and forest management is central to evaluating regeneration outcomes under changing environmental conditions [4,5].

Forest structural complexity is increasingly recognized as a key attribute of ecosystem functioning and biodiversity [6–8]. Structural heterogeneity influences microclimatic buffering, habitat availability, and ecological resilience, and cannot be fully described by single stand parameters such as basal area or mean height [7,8]. During early regeneration phases, structural differentiation emerges from interactions among species-specific growth strategies, competition for light and nutrients, and disturbance regimes. Quantifying these structural properties in a robust and comparable manner remains a methodological challenge, particularly at spatial scales relevant to browsing ungulates.

Recent advances in remote sensing, especially LiDAR-based approaches, have substantially improved the capacity to quantify three-dimensional forest structure [4,9–11]. LiDAR-derived metrics allow assessment of vertical stratification, canopy architecture, and spatial heterogeneity beyond traditional field measurements [4,10]. Fractal-based approaches, including box-dimension analysis, capture emergent stand properties by describing how vegetation occupies three-dimensional space [11]. At the same time, field-based methods such as visual obstruction measurements provide complementary information on vegetation density and concealment within specific height layers relevant to ungulate behaviour. Integrating field-based and LiDAR-derived metrics therefore offers the potential to assess forest structure from both architectural and perspective-based viewpoints.

Ungulate browsing is widely recognized as a major driver of regeneration dynamics and structural development in temperate forests, yet the relative importance of regional site conditions, species composition, and management regimes for three-dimensional forest structure remains insufficiently resolved, particularly across heterogeneous landscapes. While recent advances in LiDAR-based remote sensing enable detailed quantification of forest structural complexity, it is still unclear to what extent management-related variables such as hunting regime or fencing exert consistent effects compared to environmental

gradients and successional processes. Therefore, the aim of this study was to disentangle the relative contributions of regional, temporal, and management-related drivers to forest structural complexity and visual obstruction within the browsing-relevant height layer. To achieve this aim, we combined field-based octant silhouette measurements with LiDAR-derived box-dimension metrics and addressed three objectives: (H1) to test whether regional and species-related factors significantly influence structural complexity and visual obstruction; (H2) to assess whether structural complexity changes over time across regions as an expression of successional development; and (H3) to evaluate whether management-related variables exert weaker and less consistent effects than regional and temporal drivers.

2. Materials and Methods

The data analyzed in this study were collected within the framework of the long-term research projects Biodiversity and Ungulate Management in Managed Forests (BioWild) and its continuation Wild–Forest–Innovation (WiWaldI). Both projects aim to investigate the effects of ungulate browsing on forest regeneration under different hunting regimes across managed temperate forests in Germany. Ungulate community in the study regions.

The ungulate community within the study areas comprises several species that may influence forest regeneration to varying degrees. Roe deer (*Capreolus capreolus*) represents the most widespread and abundant browser across all regions and is considered the primary species affecting the investigated vegetation layer. In addition, red deer (*Cervus elaphus*) and wild boar (*Sus scrofa*) occur in many areas, while fallow deer (*Dama dama*) is present locally. Regionally restricted species include mouflon (*Ovis gmelini musimon*) and, rarely, sika deer (*Cervus nippon*) in parts of Saxony-Anhalt, as well as chamois (*Rupicapra rupicapra*) with low densities in Baden-Württemberg. The densities of these species vary locally depending on habitat conditions, landscape structure, hunting management, and disturbance regimes. Consequently, browsing pressure on regeneration is spatially heterogeneous and reflects the combined influence of species composition and management context Data were collected in multiple federal states representing a wide range of forest types and site conditions, including Baden-Württemberg, Brandenburg, Mecklenburg–Western Pomerania, North Rhine–Westphalia, Saarland, Saxony-Anhalt, and Thuringia (Figure 1).

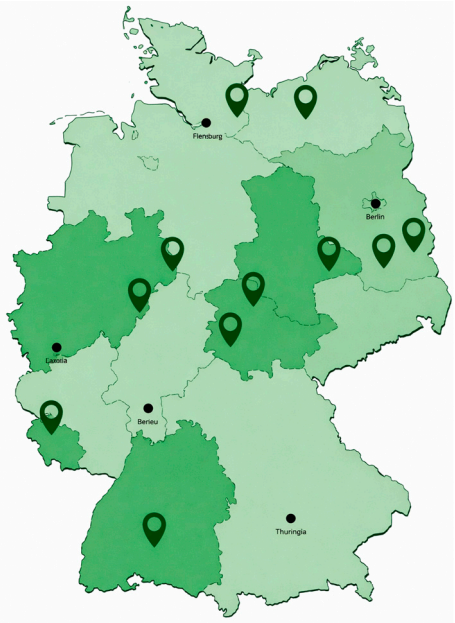

Figure 1. Locations of the paired inventory plots established within each study region.

The dominant forest types vary regionally, with European beech (*Fagus sylvatica*) prevailing in most regions, while Norway spruce (*Picea abies*) dominates in North Rhine–Westphalia and Scots pine (*Pinus sylvestris*) in Brandenburg (Table 1).

Table 1. Study regions in Germany included in the WiWaldI project with dominant forest communities and sampling intensity.

Study Regions	Dominant Forest Community	Number of Inventory Plot (Plot Pair)
Baden-Württemberg	Montane mixed forest with silver fir	83
Brandenburg	(Sessile oak) pine forest	12
Mecklenburg–Western Pomerania	Woodrush–European beech forest	6
North Rhine–Westphalia	Norway spruce plantations	50
Saarland	Woodrush–beech forest with sessile oak	30
Saxony-Anhalt	Pine plantations and woodrush–beech forest	73
Schleswig-Holstein	Beech forest communities	22
Thuringia	Wood barley–beech forest with noble hardwood species	12

Inventory plots were selected based on region-specific model predictions of the probability of natural regeneration derived from site and stand variables [10]. Hereafter, the term inventory plot is used synonymously with plot pair and refers to the paired fenced–unfenced sampling unit established at each selected location. Because not all predictors of the original model were available across all regions, a simplified model was re-parameterized using data from the third German National Forest Inventory, meteorological records, and soil information. Potential plot-pair locations were identified using a 200 m grid in ArcMap version 10.6 (released in 2018; Esri Inc., Redlands, CA, USA), and grid points were ranked according to predicted regeneration probability; the number of plot pairs per hunting district was allocated proportionally to district size (≈1 plot pair per 100 ha). The selected areas were thus characterized by representing stands with expected regeneration potential while ensuring identical stocking and light conditions between the fenced reference plot and the unfenced comparison plot within the study areas. In the field, sites were accepted only if regeneration height was $\leq$50 cm and if both subplots showed comparable soil, water availability, ground vegetation, stand structure, aspect, and topography. Each inventory plot (plot pair) consisted of one fenced and one unfenced plot (12 $\times$ 12 m), located 5–20 m apart within the same forest stand, with fenced plots serving as reference areas without ungulate influence and unfenced plots exposed to natural browsing pressure (Figure 2). On the unfenced comparison plots of each exclosure pair, representing the areas under ungulate influence, the silhouette and octant surveys were conducted. Roads, skid trails, and locations with evident structural disparities were excluded to maintain a strictly rule-based selection.

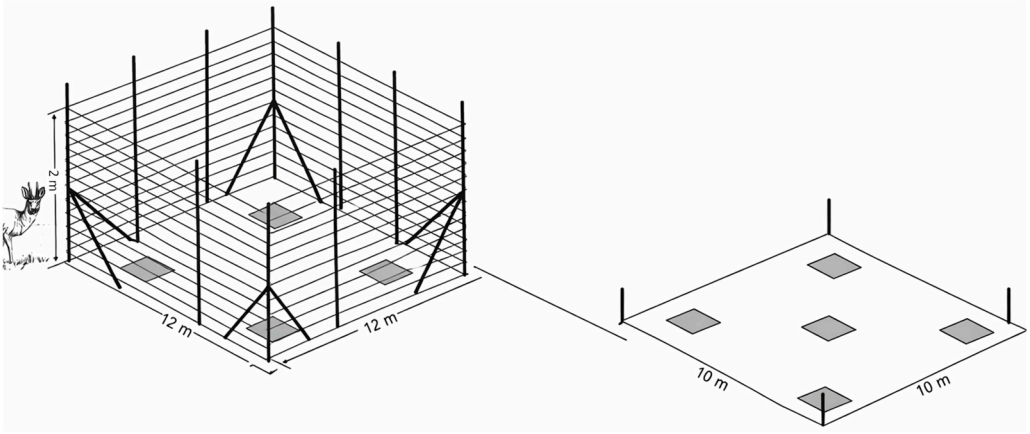

Figure 2. Pair of monitoring plots. Adapted from: Reimoser and Suchant (1992) [12]. Five 4 m^2 subplots are indicated in grey color. Within exclosures, the same area was investigated as outside (10 × 10 m).

All study areas were subject to active hunting management and were classified into three hunting regimes (A, B, and C). Assignment to hunting regimes was based on the assessment of the respective holders of the hunting rights. Hunting regime A represents areas with ungulate populations considered high relative to site conditions, whereas hunting regime B includes areas with populations regarded as adapted to the habitat. In both regimes, the existing hunting strategy was maintained to preserve the current population status. In contrast, hunting regime C involved an active modification of the hunting strategy aimed at achieving a site-adapted ungulate population, with a focus on increasing hunting efficiency while reducing disturbance and shortening hunting periods. No direct ungulate density estimates were collected within this study. Wildlife counts were not conducted because local population levels may vary considerably in response to habitat composition and site-specific carrying capacity. Density figures alone do not necessarily reflect actual browsing pressure and can therefore be misleading when interpreted without ecological context. The study focused instead on the condition of the vegetation, particularly woody regeneration, as an integrative indicator of ungulate influence on forest development. The paired fenced–unfenced design enabled a direct comparison between areas with and without browsing impact and allowed the separation of effects attributable to ungulates from those resulting from intraspecific plant competition and successional dynamics. This approach ensured that the evaluation of browsing impact was based on observable vegetation responses rather than on uncertain density estimates. Data collection for this study was conducted using two complementary methods, which are described in the following sections. The longitudinal vegetation surveys conducted throughout the project duration enabled us to cross-check the declared hunting regime classification against observed regeneration patterns and browsing indicators. This empirical validation allowed us to assess whether the practical implementation of the respective management strategy and the resulting vegetation conditions were consistent with the stakeholder-based regime assignment.

2.1. Octant-Based and Silhouett Vegetation Sampling

Structural parameters describe habitat suitability for ungulates not only in terms of forage availability but also with respect to cover and visibility [11]. Limited cover increases the visibility of individuals and is associated with larger Browsing areas and lower local densities [13–15], whereas sufficient cover allows higher densities of roe deer to persist within the same area [16]. Consequently, cover availability represents a major limiting factor for roe deer populations [17]. To assess habitat development with respect to structure

and cover, we analysed 248 permanent unfenced observation monitoring plots in addition to standard vegetation surveys. During the main growing season (June–August), structural vegetation development and ungulate effects were monitored on these plots. Browsing and concealment capacity were quantified using the Octant & Silhouette method [18], which was developed to capture gradients in habitat capacity from an animal-centred perspective and provides standardized structural indicators for characterizing habitat quality for ungulates. The approach is suitable for application by practitioners in forest management, while the silhouette component enables quantitative assessment of visual cover.

For this method, a permanent circular sampling area with a radius of 25 m (approximately 1963 m^2) was established on each unfenced plot, centred on the permanent inventory plot (Figure 3). The circular area was divided into eight equal octants. In each octant, the woody plant closest to the plot centre with a height between 80 and 200 cm was recorded, representing the browsing-relevant vegetation layer. The lower threshold corresponds to the average shoulder height of roe deer, while the upper limit reflects the maximum browsing height of larger ungulate species. Distances between the plot centre and selected plants were measured using an ultrasonic Vertex IV-GS device with a T3 transponder (Haglöf, Stockholm, Sweden). For each plant, species identity, horizontal and vertical crown extension, and visible signs of ungulate impact (browsing) were recorded. The number of occupied octants and the mean distance of woody plants from the plot centre served as indicators of structural availability and potential cover, with higher octant occupancy and shorter distances indicating greater habitat quality in terms of visual protection.

$$\overline{D} = (1/n)\ \sum_(i = 1)\hat{}n\ d_i, \text{with } n = \text{numberofoccupiedoctants.}$$

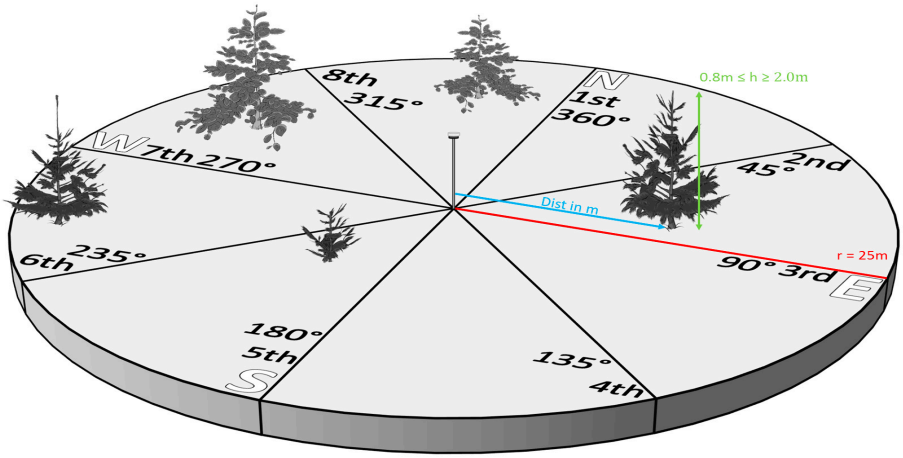

Figure 3. Octant Plot with a radius of 25 m divided into eight octants. Edge trees span the ungulate area of influence.

Octant occupancy O, mean distance to woody plants $\overline{D}$ as well as species and damage records were derived from the octant survey. For each octant i = 1…8, the octant was classified as unoccupied (O_i = 0) if no woody plant within the height class of 80–200 cm was present, or as occupied (O_i = 1) when at least one suitable plant occurred. For occupied octants, the distance d_i from the plot centre P to the selected plant was measured using a Vertex IV-GS ultrasonic device with a T3 transponder.

It is acknowledged that forest development is not solely dependent on ungulate influences but is also determined by forest stand type, site characteristics, and light conditions. The silhouette-based method quantifies visual cover using a life-size silhouette of two roe deer (doe and fawn). Roe deer represents the most widespread and frequently occurring wild ungulate species of this body size in Central Europe [19] and depends strongly on visual cover as a key habitat requirement [20]. For each plant previously identified using the

octant method, the silhouette was positioned directly behind the plant and photographed under standardized conditions (Figure 4). Visual obstruction was recorded using a digital camera with interchangeable lens (Sony SAL1855 lens (Sony Corporation, Tokyo, Japan)). The focal length was set to 18 mm. The camera was positioned at a height of 1.10 m above ground and aligned frontally to the target area, with a horizontal distance of 1.30 m between the camera and the vegetation. Camera model (Sony SAL1855), distance, height, lens type, and magnification were kept constant across all measurements to ensure a standardized geometry and a consistent field of view covering both the vegetation layer and the ungulate silhouette zone. Visual cover was quantified as the proportion of the silhouette obscured by plant structures using pixel-based analysis conducted in Adobe Photoshop CC 2018 (Adobe Inc., San Jose, CA, USA), with camera model, distance, height, lens type, and magnification kept constant across all measurements to ensure a standardized geometry and a consistent field of view. To minimize errors caused by shadows, reflections, and variable lighting conditions, images were manually processed, allowing accurate identification of plant-covered silhouette areas. All image processing steps were conducted by a single trained operator following a predefined and standardized workflow to ensure consistency across all sampling years. Although manual segmentation may involve a degree of subjectivity, applying identical criteria throughout the study period establishes methodological consistency and reduces inter-observer variability, resulting in systematic rather than random error across the dataset. Despite standardized procedures and quality control, pixel-based segmentation inherently involves operator-dependent decisions, particularly in distinguishing fine branches, shaded areas, or partially occluded silhouette sections, which may introduce minor classification variability. To ensure completeness and exclude systematic misclassification, random subsamples were independently checked by a second person, confirming consistent and comprehensive pixel assignments, including shaded woody structures and foliage covering the standardized roe deer silhouette. Visual cover was expressed as the percentage of the silhouette area covered by vegetation, providing a standardized measure of concealment from an ungulate perspective.

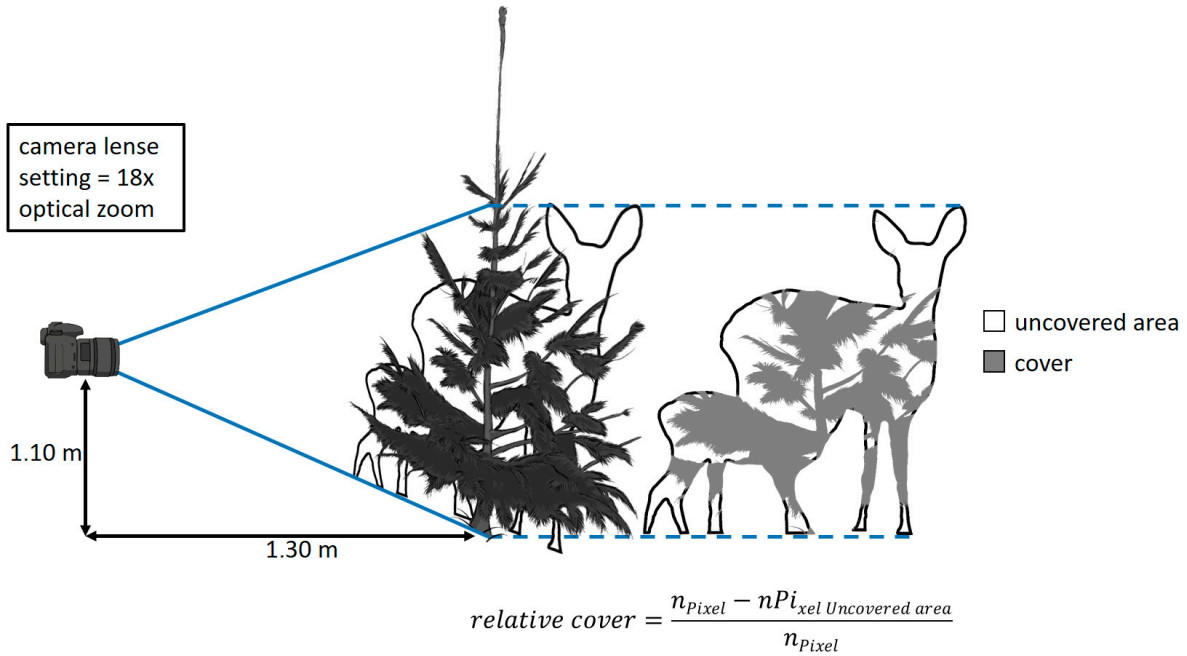

$$relative\ cover = \frac{n_{Pixel} - nPi_{xel\ Uncovered\ area}}{n_{Pixel}}$$

Figure 4. Recording of roe deer silhouette coverage as an index of habitat structure on unfenced study plots.

2.2. Laser Scanning

The scanning of the fenced and unfenced sample plots was carried out using the handheld laser scanning system ZEB-Revo (GeoSLAM Ltd., Nottingham, UK). Handheld LiDAR scanners are characterized by their compact design and low weight, enabling operation by a single person without the need for extensive infrastructure. This makes them particularly suitable for surveys in difficult-to-access, confined, or rough terrain and for the assessment of complex forest structures such as dense thickets. As positioning and data registration are primarily based on SLAM algorithms, data acquisition does not depend on satellite-based GNSS connectivity. Consequently, start and end points can be reliably linked even in shielded or topographically challenging forest sections, allowing the generation of complete point clouds independent of external georeferencing. Each sub-plot was first traversed along a diagonal and subsequently covered in loops spaced approximately 2.5 m apart. Data were transferred from the scanner data logger to the computer via USB. The point clouds were processed using Geoslam Hub (GeoSLAM Ltd., Nottingham, UK) and converted into LAZ files, which were imported into the 3D point-cloud software CloudCompare (CloudCompare version 2.13 alpha) (www.cloudcompare.org). The point clouds were trimmed to the actual size of the sample plots, and fence fragments protruding into the data due to slope inclination or misalignment were removed after visual inspection. The individual plots were then smoothed by reducing the point density to a resolution of 10 cm. A resolution of 10 cm was selected as a conservative estimate of the reliably available spatial resolution within the processed point clouds. While coarser resolutions of approximately 20 cm are commonly applied in mobile laser scanning studies when full canopy structure is considered and occlusion effects need to be minimized, the present study focused exclusively on the forest understory (<2 m height). Within this lower vegetation layer, occlusion is substantially reduced due to the close proximity of the handheld sensor to the scanned structures. The 10 cm resolution therefore reflects a confidence-based compromise between preserving fine-scale structural information and ensuring robustness against potential occlusion artifacts. To improve comparability, a slope correction was applied to the thinned data, and all points above 2 m were clipped to represent the upper limit of ungulate browsing influence. Based on the finalized point clouds, fractal dimensions were calculated as a measure of structural complexity. The box-counting dimension ($D_{(b)}$) was derived following Seidel (2018) [21] using a lower cut-off of 10 cm. The box dimension represents a quantitative measure of the three-dimensional structural complexity of vegetation, describing how densely point-cloud information occupies space across multiple spatial scales. Higher values indicate a more heterogeneous and vertically differentiated structure with greater branching and layering, whereas lower values reflect simplified, sparsely structured vegetation. The parameter integrates information on stem density, crown architecture, and vertical stratification into a single metric and is sensitive to changes in regeneration development and browsing impact (Figure 5).

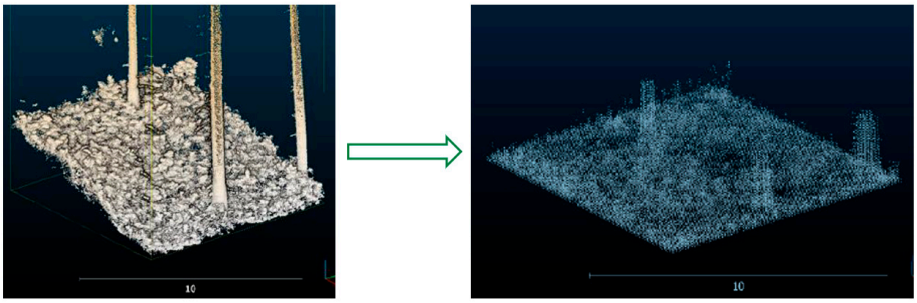

Figure 5. Point cloud of a sub-plot following trimming (**left**) and after surface smoothing and slope correction (**right**).

2.3. Statistical Analysis

RStudio (version 2024.12.0) was used to analyze the data using the R version 4.2.0 (2022-04-22)—"*Vigorous Calisthenics*" R Core Team (2022). Initially, the descriptive statistical parameters minimum, maximum, mean, median, variance, and standard deviation were calculated for the visual obstruction coverage (SD) and box dimension ($D_{(b)}$) values. Subsequently, the normality of SD and $D_{(b)}$ values was assessed using graphical methods. To ensure normal distribution, the plot M5_03_01 was excluded from further analyses, as it exhibited an exceptionally low $D_{(b)}$ value in 2023. Following this adjustment, multifactorial analyses of variance (ANOVA) were conducted to test the effects of the variables federal state, hunting regime, fencing, and dominant tree species on visual obstruction coverage and box dimension. Significant effects were further examined using Tukey's HSD post hoc tests. As distance values were not normally distributed, which was additionally confirmed using the Shapiro–Wilk test, non-parametric Kruskal–Wallis tests were applied. In cases of significant results, Dunn's post hoc tests were subsequently performed. Spearman rank correlation tests were used to assess relationships between individual variables. The two datasets were merged in R, allowing relationships between SD and $D_{(b)}$ to be analyzed. For graphical visualization, the R version 4.2.0 (2022-04-22) within RStudio (version 2024.12.0) was used. To improve visualization of the relationship between visual obstruction coverage and distance to the plot center in the two survey years (Figure 3), the data were aggregated by calculating mean values of the eight individual measurements per plot. Consequently, each plot was represented by a single SD and distance value. Furthermore, for the analysis of the fencing effect on structural complexity, seventeen plots were excluded from the dataset due to detected gate defects. As a result, protection against ungulate browsing was no longer ensured on these plots, and the function of the exclosure as a control plot was no longer fulfilled.

3. Results

The results are presented for the two main response variables, visual obstruction coverage (SD) and LiDAR-derived structural complexity ($D_{(b)}$), and are structured in relation to the three hypotheses outlined in the Introduction. Analyses were conducted for the survey years 2019 and 2023. The pilot region Schleswig-Holstein was excluded, as it has been part of the WiWaldI project only since 2024. No data were available for Brandenburg and Mecklenburg–Western Pomerania in 2019. Federal state was included as a categorical factor in the statistical model.

3.1. Results of the Octant Silhouette Method

Tree species composition derived from the octant silhouette method is shown in Figure 2. Each recorded plant corresponds to one occupied octant. Across all federal states, the total number of occupied octants declined in 2023 compared to 2019. The smallest absolute reduction occurred in Baden-Württemberg (−13 octants), while the largest decreases were observed in Saxony-Anhalt (−146) and North Rhine–Westphalia (−151). In relative terms, Thuringia exhibited the strongest decline (−49.5%).

For further analyses, maple species were grouped as *Acer* spp. and oak species as *Quercus* spp. Baden-Württemberg recorded the highest number of occupied octants in both years (543 in 2019; 530 in 2023). *Fagus sylvatica* was dominant in both years and increased in relative share. In Brandenburg, *Pinus sylvestris* dominated (60.6%), followed by *Quercus* spp. (33.7%). In Mecklenburg–Western Pomerania, *Fagus sylvatica* was most frequent (35%), with *Pinus sylvestris*, *Pseudotsuga menziesii*, and *Quercus* spp. represented in similar proportions. North Rhine–Westphalia showed a marked reduction in occupied octants (−48.2%), accompanied by an increased relative importance of *Fagus sylvatica*.

Saarland remained dominated by *Fagus sylvatica*, while Saxony-Anhalt showed a decline in its relative share and an increase in other broadleaved species. In Thuringia, other broadleaved species dominated in 2019, whereas *Fagus sylvatica* became dominant in 2023 (Figure 6).

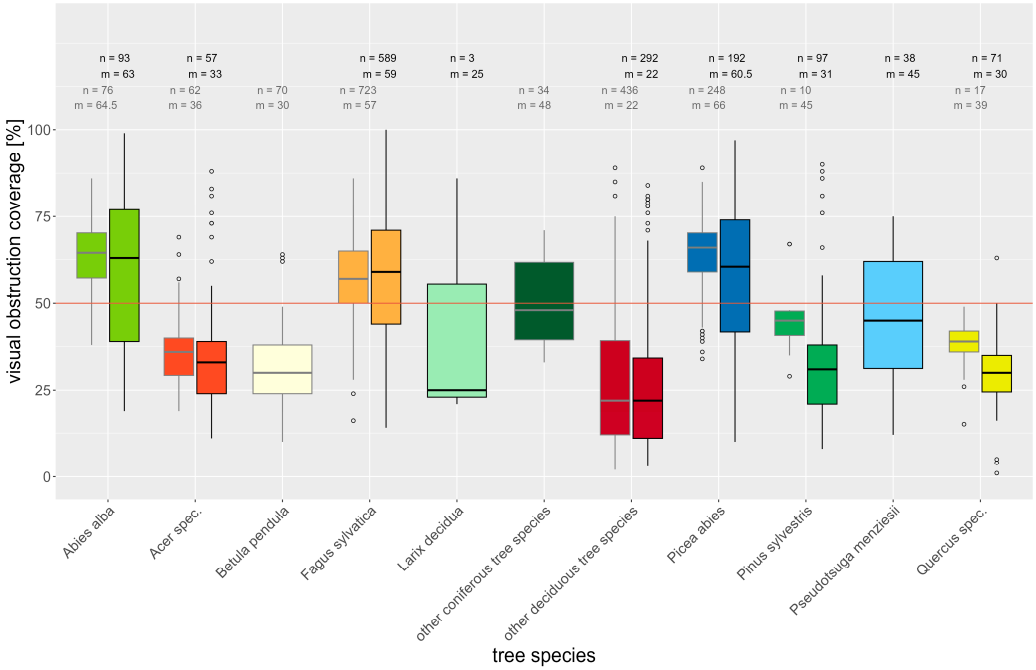

Figure 6. Visual obstruction coverage (%) of tree species. Light-colored bars represent data from 2019, whereas dark-colored bars represent data from 2023.

The distribution of visual obstruction coverage across tree species and height classes is shown in Figure 7 (2019) and Figure 8 (2023). As in Figure 3, Norway spruce (*Picea abies*), silver fir (*Abies alba*), and European beech (*Fagus sylvatica*) exhibited the highest mean visual obstruction coverage, whereas other broadleaved species showed the lowest values. Within most species, differences among height classes were small. In silver fir, variability decreased in the upper height classes (161–180 cm and 181–200 cm), while in other broadleaved species mean visual obstruction coverage was highest in the 181–200 cm class. Differences among height classes were minor for silver birch (Betula pendula), maple species (*Acer* spp.), and oak species (*Quercus* spp.). Scots pine (*Pinus sylvestris*) showed comparatively high visual obstruction coverage in the 101–120 cm class and a markedly greater variability across height classes. In other coniferous species, visual obstruction coverage was slightly higher in the 121–140 cm and 161–180 cm classes. In 2023, the same species exhibited the highest and lowest visual obstruction coverage, but European beech, silver fir, and Norway spruce covered a wider range of values than in 2019. Height-class differences remained small in European beech. In Norway spruce, the 161–180 cm class showed a higher median and lower variability, while silver fir displayed stronger differentiation, with lowest mean values in the 80–100 cm class and increasing values up to 121–140 cm, followed by reduced variability in the upper classes. In maple species, Scots pine, and Douglas fir (*Pseudotsuga menziesii*), the highest height class exhibits the lowest visual obstruction coverage in 2023.

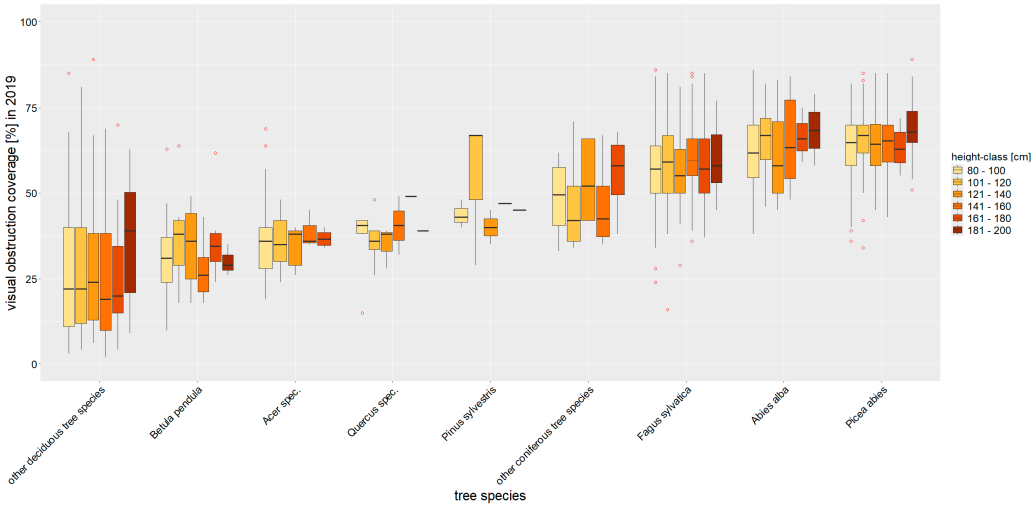

Figure 7. Visual obstruction coverage (%) of tree species by height classes in 2019.

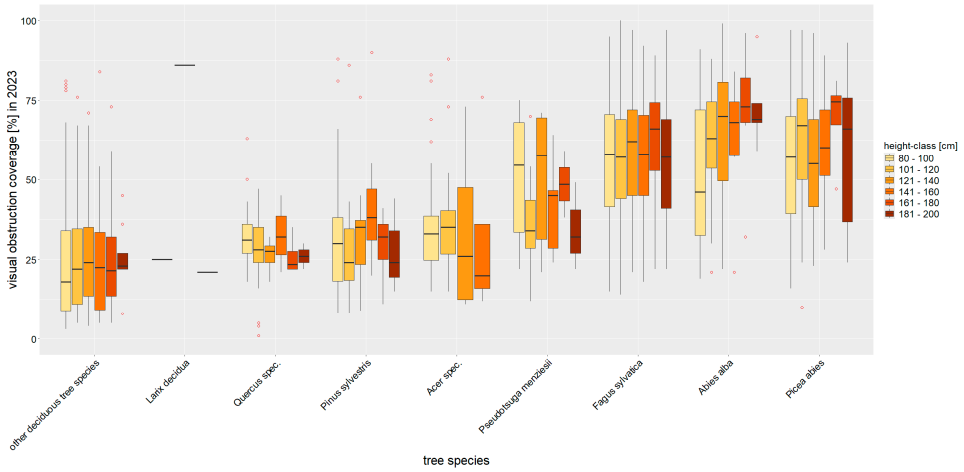

Figure 8. Visual obstruction coverage (%) of tree species by height classes in 2023.

An overview of visual obstruction coverage for 2019 and 2023 across pilot regions and hunting regimes is presented in Figure 9. All hunting regimes were represented in Baden-Württemberg, Brandenburg, North Rhine-Westphalia, and Saarland, whereas only regime B occurred in Mecklenburg–Western Pomerania, regimes A and C in Saxony-Anhalt, and regime C in Thuringia. An increase in mean visual obstruction coverage from 2019 to 2023 was observed only in Baden-Württemberg and marginally in North Rhine-Westphalia under regime A; in all other cases, coverage declined. Median values varied substantially among federal states and regimes. The highest medians were recorded in Baden-Württemberg under regime B in 2023 (67%), North Rhine-Westphalia under regime C in 2019 (58%), and Saarland under regime A in 2019 (62%). In contrast, Brandenburg consistently exhibited the lowest median values across regimes, ranging from 22% (C, 2023) to 34% (A, 2023), and showed comparatively low variability. The lowest recorded value occurred in Brandenburg under regime B in 2023 (1%), whereas the maximum value of 100% was observed in Saxony-Anhalt under regime C in 2023. Thuringia displayed median values below 40% in 2023 but included several higher individual observations, while Baden-Württemberg and Saxony-Anhalt covered broader value ranges overall. Sample sizes varied considerably among boxplots, ranging from eight observations in Saarland (A, 2023) to 479 in Saxony-Anhalt (C, 2019). Across regimes, Saarland showed comparatively high values under regime A, Baden-Württemberg under regime B in 2023, and North

Rhine-Westphalia under regime C in both years. Overall, Brandenburg exhibited the lowest mean visual obstruction coverage across hunting regimes.

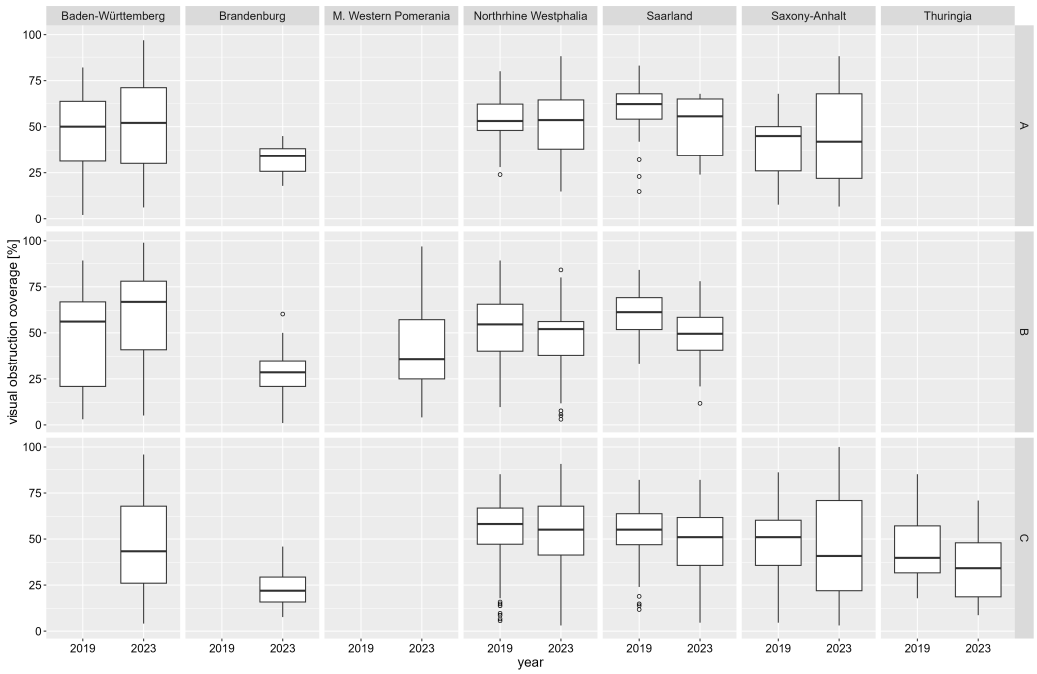

Figure 9. Visual obstruction coverage (%) in 2019 and 2023 across federal states and hunting regimes A, B and C.

In both 2019 ($p = 1.30 \times 10^{-5}$) and 2023 ($p = 2.19 \times 10^{-7}$), federal state had a significant effect on visual obstruction coverage, although not all pairwise comparisons were significant. Federal state was included as a categorical variable representing differing silvicultural site conditions. In 2019, most federal states differed significantly from one another, with the exception of Saxony-Anhalt, which did not differ from Baden-Württemberg or Thuringia, and Saarland, which did not differ from North Rhine-Westphalia. In 2023, differentiation among federal states was more pronounced. Brandenburg differed significantly from all other states except Thuringia, while Mecklenburg–Western Pomerania showed significant differences only relative to Baden-Württemberg and Brandenburg. Additional significant differences were observed among several central German states, whereas some comparisons remained non-significant. Across models, federal state showed statistically significant effects in both years, whereas hunting regime did not show significant effects. Hunting regime had no significant overall effect on visual obstruction coverage in 2019 ($p = 0.242$) or 2023 ($p = 0.294$). Although isolated pairwise contrasts were detected in 2023, no consistent differences among hunting regimes were observed. Across models, management-related variables did not consistently explain variation in visual obstruction coverage. Distance to the plot center by year, federal state, and hunting regime is shown in Figure 10. Most outliers occurred above the upper quartile. Distributions were largely comparable across hunting regimes within federal states. In several regions, including Baden-Württemberg and North Rhine-Westphalia, the first three quartiles were generally below 12 m, with increasing variability in the upper quartile. Brandenburg, Mecklenburg–Western Pomerania, and Thuringia showed comparatively low variability. No systematic differences in distance to the plot center or dispersion patterns were observed among hunting regimes.

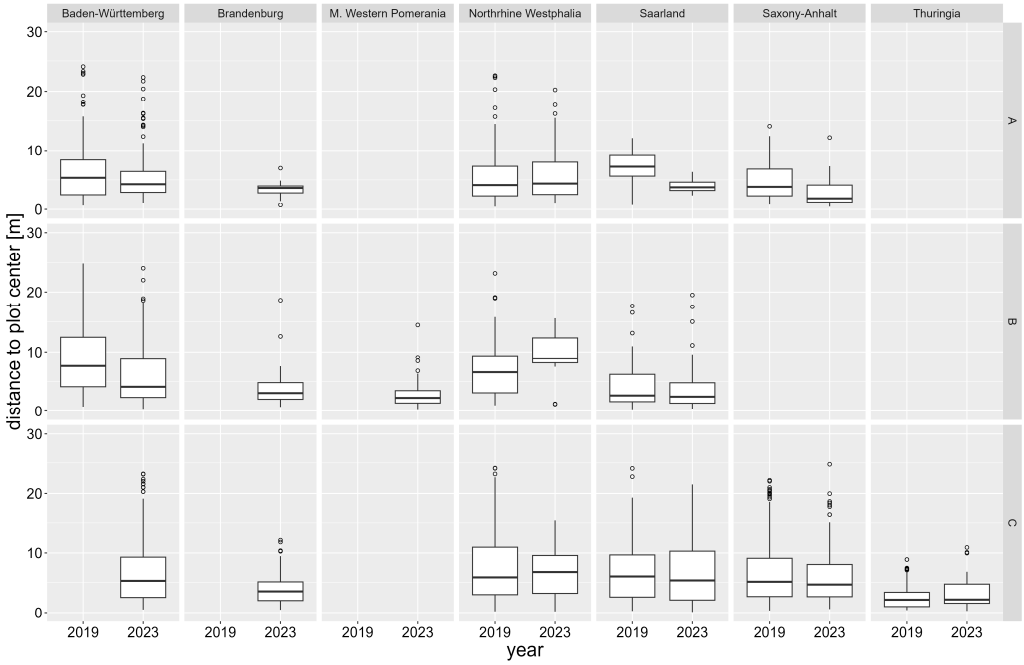

Figure 10. Distance to the plot center (m) in 2019 and 2023 across federal states and hunting regimes A, B, C.

The regression lines shown in red in Figure 11 indicate contrasting relationships between mean visual obstruction coverage and mean distance to the plot center among federal states.

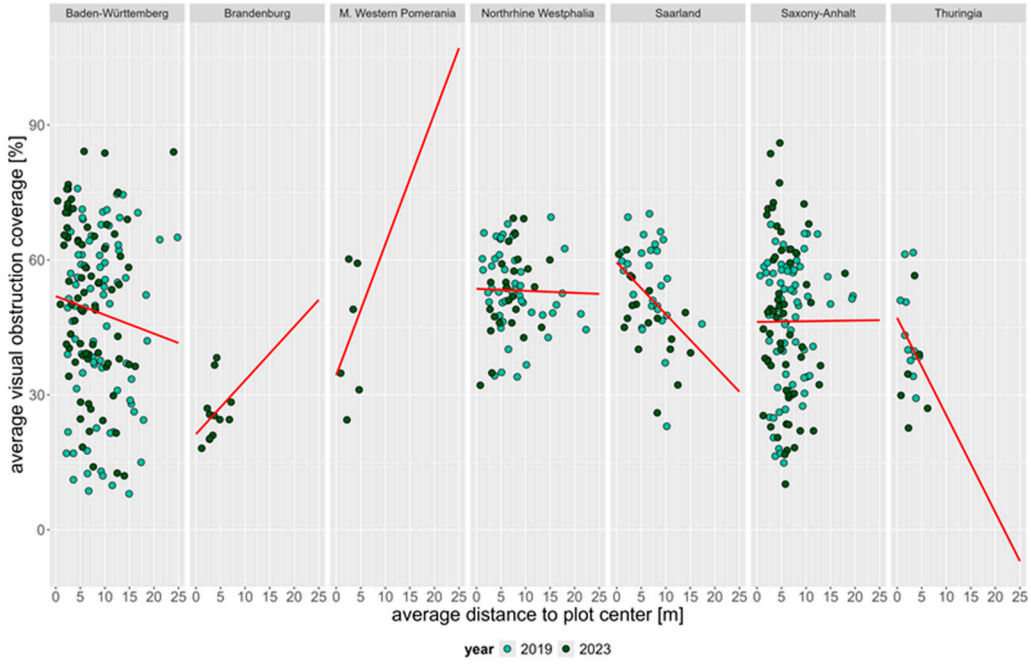

Figure 11. Mean visual obstruction coverage (%) as a function of mean distance to the plot center (m) across federal states in 2019 and 2023, with regression lines shown in red.

A negative association was observed in Baden-Württemberg, North Rhine-Westphalia, Saarland, and Thuringia, with the strongest slopes in Saarland and Thuringia and a comparatively weak pattern in North Rhine-Westphalia. In contrast, Brandenburg, Mecklenburg–Western Pomerania, and Saxony-Anhalt exhibited positive slopes, which were pronounced in Brandenburg and Mecklenburg–Western Pomerania and weaker in Saxony-Anhalt.

Mean visual obstruction coverage was not significantly related to mean distance to the plot center in 2019 ($p = 0.531$) or 2023 ($p = 0.162$). When observations from both years were pooled, a weak but significant correlation was detected ($p = 0.00896$). Visual obstruction coverage spanned the full range from 1 to 100% across all explanatory variables. In contrast, visual obstruction coverage showed a significant positive relationship with plant height when data from both years were combined ($p < 2.2 \times 10^{-16}$), although this relationship was not significant in 2023 (Figure 12). Plant width and the height-to-width ratio exhibited strong and consistently significant positive relationships with visual obstruction coverage in both individual years and in the pooled dataset.

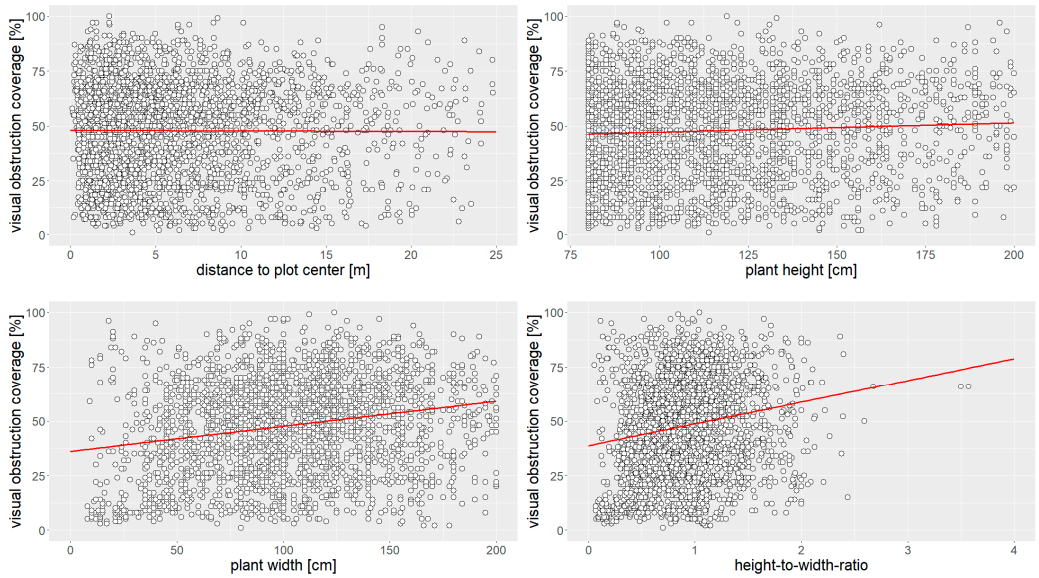

Figure 12. Relationships between visual obstruction coverage (%) and distance to plot center, plant height, plant width, and height-to-width ratio. Red lines indicate fitted trends. Spearman's rank correlation coefficients (ρ) and *p*-values are reported in the text.

3.2. Box Dimension Analysis

Changes in box-dimension-based structural complexity between 2019 and 2023 across federal states are shown in Figure 13. All federal states with data for both years exhibited an increase in complexity over time. In 2019, median values were similar among Saarland (1.70), North Rhine-Westphalia (1.71), Baden-Württemberg (1.72), and Saxony-Anhalt (1.72), while Thuringia showed slightly higher values (1.77).

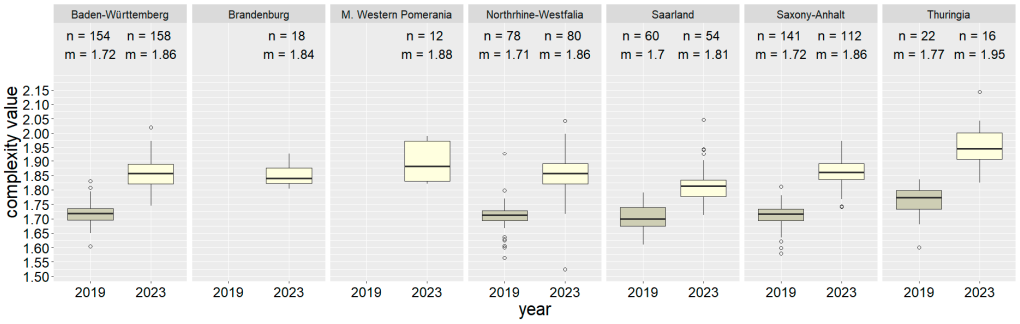

Figure 13. Complexity values in the pilot regions for the survey years 2019 and 2023.

By 2023, complexity increased in all regions. Saarland showed the lowest median (1.81) despite an increase of 0.11. Baden-Württemberg and Saxony-Anhalt increased by 0.14 to 1.86, and North Rhine-Westphalia increased by 0.15 to the same level. Brandenburg (1.84)

and Mecklenburg–Western Pomerania (1.88) exhibited similarly high values. Thuringia showed the largest increase (+0.18) and reached the highest median overall (1.95). Federal state significantly affected structural complexity in both 2019 ($p = 9.11 \times 10^{-5}$) and 2023 ($p < 2.2 \times 10^{-16}$), with stronger differentiation in 2023. In 2019, only Thuringia differed significantly from all other federal states. In 2023, Thuringia again showed significantly higher complexity than all states except Mecklenburg–Western Pomerania, while Saarland differed from all others except Brandenburg. These results indicate statistically significant differences in structural complexity among federal states. Structural complexity increased between 2019 and 2023 in all regions. Differences among federal states were statistically significant, whereas hunting regime effects were not significant in either year. Complexity values of fenced and unfenced plots are also shown in Figure 13. In 2019, medians were similar between plot types in most federal states. By 2023, complexity was generally higher on exclosures than on unfenced plots, particularly in Thuringia. However, fencing had no significant effect in 2019 ($p = 0.219$). Although a significant main effect was detected in 2023 ($p = 0.017$), no significant pairwise differences between fenced and unfenced plots were observed.

In 2019, fencing had no significant effect on structural complexity ($p = 0.219$). In 2023, a significant main effect of fencing was detected ($p = 0.017$); however, no significant pairwise differences between fenced and unfenced plots were observed. Median differences varied among federal states, and the magnitude of variation remained smaller than that explained by regional effects. Complexity values by dominant tree species are shown in Figure 14. All species exhibited increases in structural complexity between 2019 and 2023 of similar magnitude (0.13–0.15). In 2023, *Acer* spp. showed the highest median complexity (1.93), followed by *Fraxinus excelsior* (1.91) and *Pseudotsuga menziesii* (1.89). *Alnus glutinosa* and *Quercus* spp. exceeded the overall 2023 mean (1.86), whereas *Fagus sylvatica*, *Larix decidua*, and *Picea abies* showed lower median values. Tree species significantly affected structural complexity in both 2019 ($p = 7.95 \times 10^{-7}$) and 2023 ($p = 0.00144$).

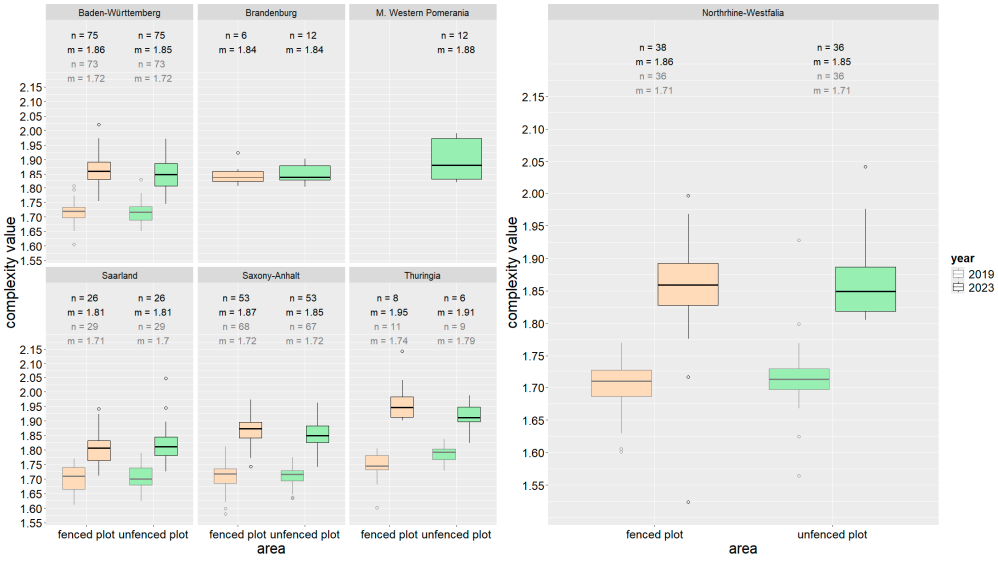

Figure 14. Complexity values of fenced and unfenced plots in the pilot regions for the survey years 2019 and 2023.

Tree species significantly affected structural complexity in both 2019 ($p = 7.95 \times 10^{-7}$) and 2023 ($p = 0.00144$). In 2019, only a limited number of pairwise differences were detected, with Acer spp. differing from several coniferous and broadleaved species, and additional differences occurring between *Pinus sylvestris* and *Fagus sylvatica*, as well as between *Quercus* spp. and both *Picea abies* and *Fagus sylvatica*. In 2023, significant pairwise differences

were largely restricted to *Acer* spp., which differed from *Abies alba*, *Fagus sylvatica*, and *Picea abies*, whereas no other species contrasts reached significance. Complexity values by hunting regime and federal state are shown in Figure 15. Across most federal states, median complexity values were similar among hunting regimes in 2019. From 2019 to 2023, structural complexity increased in all hunting regimes by comparable magnitudes (approximately 0.10–0.16). The highest median values in both years were observed in Thuringia under regime C. Within federal states, differences among hunting regimes were small, and no regime consistently showed higher complexity values across regions or years.

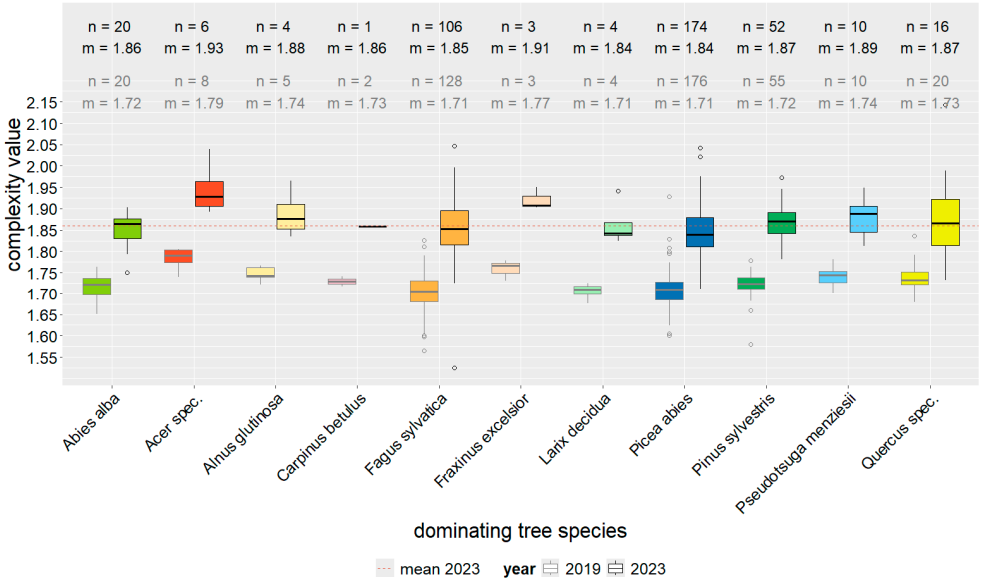

Figure 15. Complexity values of the dominant tree species in 2019 and 2023.

In 2023, no statistically significant effect of hunting regime was detected ($p = 0.0526$). In 2023, the effect approached but did not reach statistical significance ($p = 0.0526$). Differences in structural complexity between fenced and unfenced plots by year, federal state, and hunting regime are shown in Figure 16. In 2019, median differences were close to zero across most federal states and hunting regimes, with generally low variability.

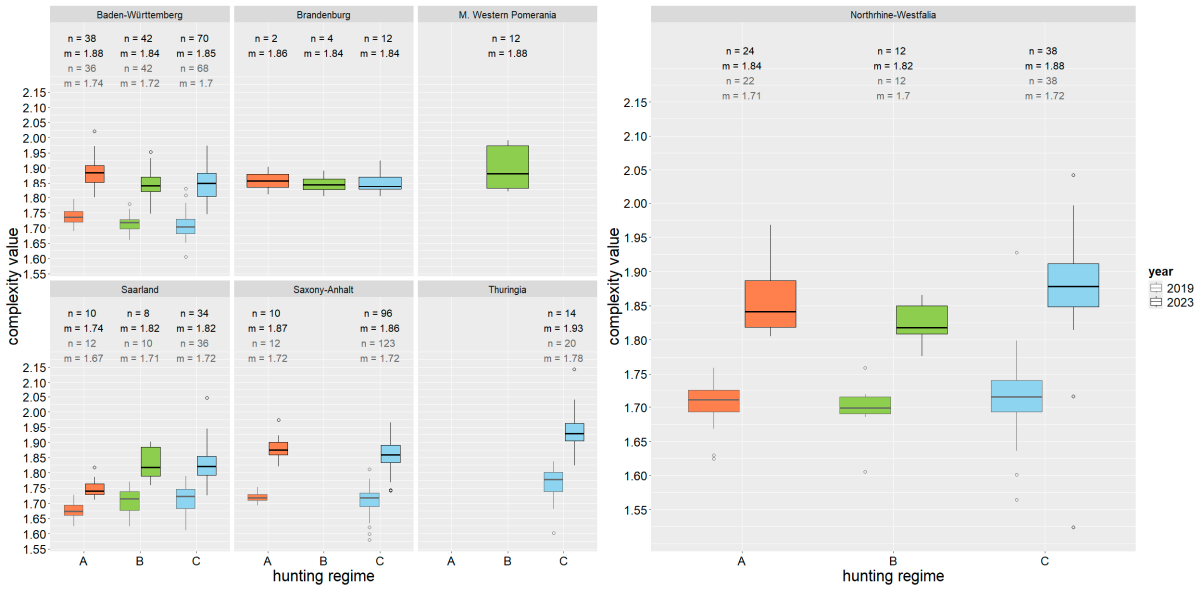

Figure 16. Complexity values of the hunting regimes in the pilot regions for the survey years 2019 and 2023.

Hunting regime A showed equal or slightly higher median differences than regimes B and C in 2019, whereas regime B tended to exhibit lower medians. Positive median differences were most frequent in Saxony-Anhalt, while negative medians were more common in North Rhine-Westphalia. In 2023, the overall range of differences increased slightly, but median values remained small and varied inconsistently among hunting regimes. The highest median difference was observed for regime C in Thuringia, whereas the lowest occurred for regime C in Saarland. Across federal states, both positive and small negative medians were recorded. Hunting regime had no significant effect on the difference between fenced and unfenced plots in 2019 ($p = 0.197$) or 2023 ($p = 0.131$), and no significant pairwise differences among regimes were detected. Federal state had no significant effect in 2019 ($p = 0.0897$), but showed a significant overall effect in 2023 ($p = 0.0199$), with Thuringia and Saarland differing significantly from each other. Differences in structural complexity of unfenced plots between 2019 and 2023 are shown in Figure 17. Overall values ranged from −0.007 (regime C in Saarland) to 0.314 (regime C in Thuringia). Although regime C displayed a wider range of differences than regimes A and B, median differences within federal states were broadly comparable among regimes.

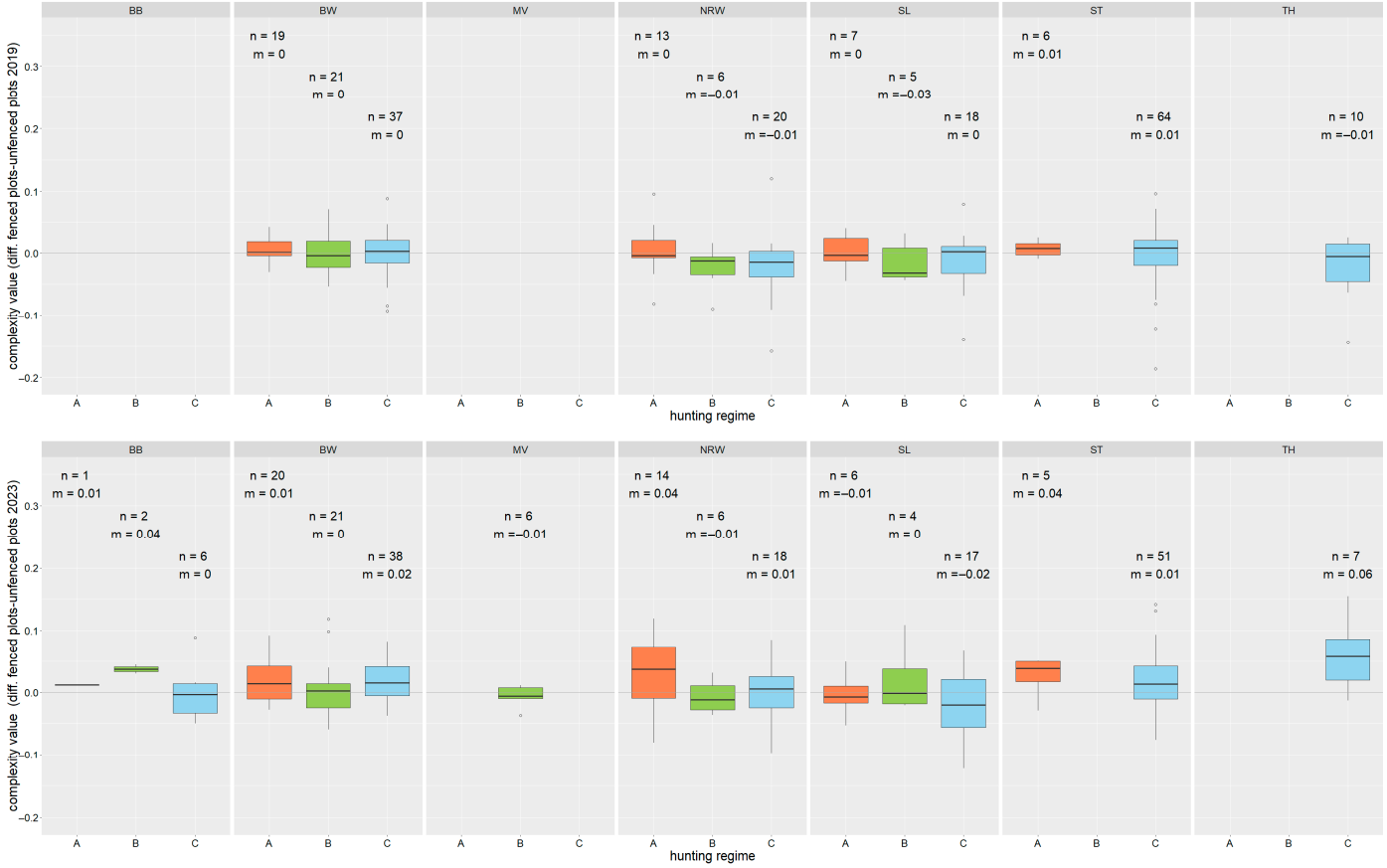

Figure 17. Difference in complexity values between fenced and unfenced plots in 2019 and 2023, stratified by hunting regimes and pilot regions.

Hunting regime had no significant effect on differences in structural complexity ($p = 0.657$), and no pairwise contrasts among regimes reached significance. In contrast, federal state showed a significant overall effect ($p = 0.00740$), although individual pairwise comparisons between federal states were not significant.

3.3. Relationship Between Visual Obstruction Coverage and Box Dimension

Figure 18 shows the relationship between mean visual obstruction coverage and structural complexity ($D_{(b)}$) in 2019 and 2023. From 2019 to 2023, the range of visual obstruction coverage increased, and complexity values were distributed at higher levels in 2023. In 2019, a significant negative relationship between visual obstruction coverage and structural complexity was detected ($p = 9.81 \times 10^{-8}$). In 2023, no significant relationship was observed ($p = 0.555$).

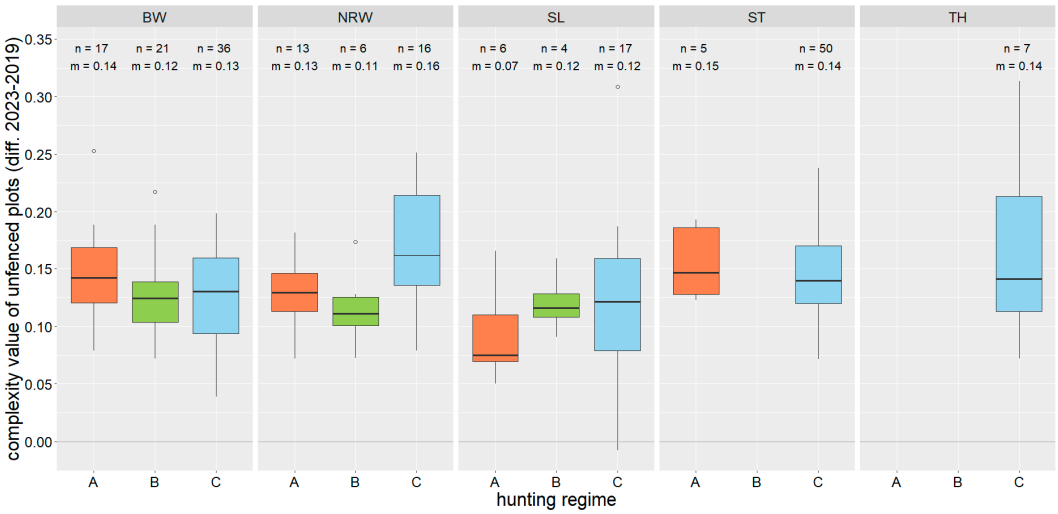

Figure 18. Difference in complexity values of unfenced plots between 2023 and 2019 across hunting regimes in the pilot regions.

3.4. Relationship Between Distance to the Plot Center and Box Dimension

Figure 19 illustrates the relationship between distance to the plot center and structural complexity ($D_{(b)}$) in 2019 and 2023. In both years, distances ranged from approximately 0.1 m to 24.8 m, with most observations below 10 m and a pronounced clustering between 0 and 5 m in 2023 (Figure 20). Structural complexity ranged from 1.62 to 1.84 in 2019 and from 1.73 to 2.05 in 2023. Regression analyses revealed a significant negative relationship between distance to the plot center and structural complexity in both years ($p < 2.2 \times 10^{-16}$).

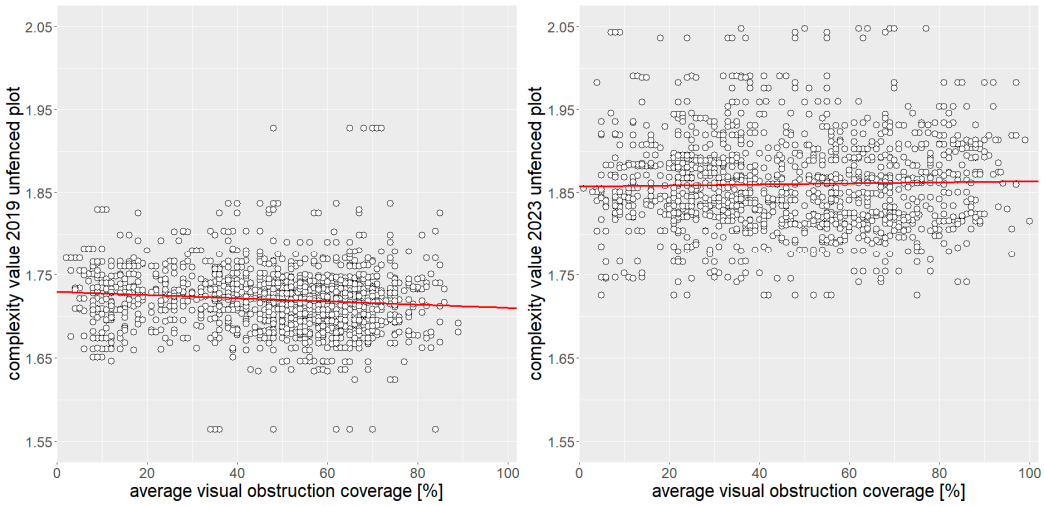

Figure 19. Relationship between mean visual obstruction coverage (%) and structural complexity ($D_{(b)}$) on unfenced plots in 2019 and 2023, with regression lines (red).

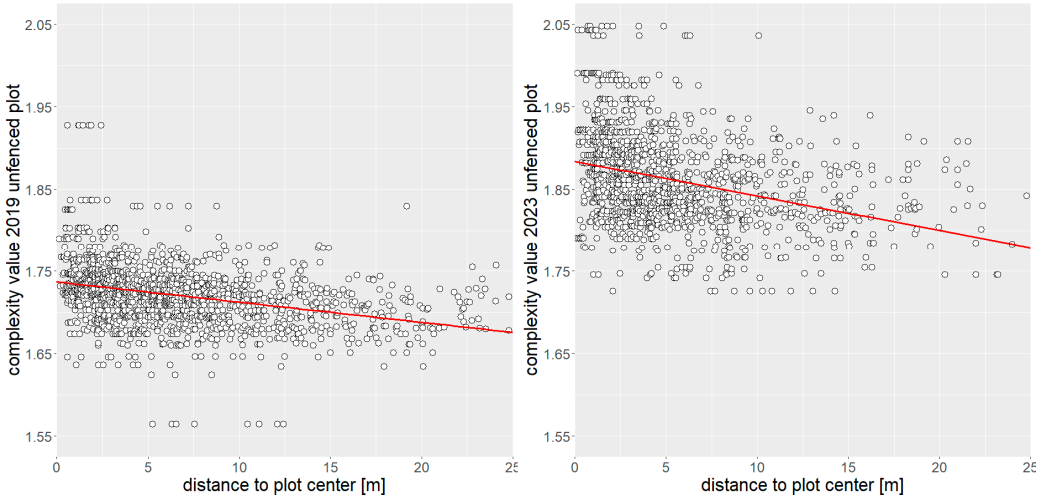

Figure 20. Relationship between distance to the plot center (m) and structural complexity ($D_{(b)}$) in 2019 and 2023, with regression lines (red).

4. Discussion

This study examined how forest structural complexity and visual obstruction vary across regions, over time, and under different management regimes. Overall, the results indicate that regional site conditions and successional development exerted stronger and more consistent effects on structural parameters than management-related variables. Hypothesis H1 was supported, as regional and species-related factors significantly influenced both structural complexity and visual obstruction. Hypothesis H2 was supported by the observed temporal increase in structural complexity. In contrast, Hypothesis H3 was confirmed in that management-related effects were generally weaker and less consistent than regional and temporal drivers. These findings emphasize the dominant role of environmental gradients and stand development in shaping regeneration structure within the studied timeframe.

4.1. Octant-Silhouette Method Results

Differences in mean visual obstruction coverage among tree species cannot be explained solely by their classification into light-demanding, intermediate, and shade-tolerant groups [22,23]. Although shade-tolerant species such as *Abies alba* and *Fagus sylvatica* exhibited comparatively high obstruction values, deviations among intermediate species indicate that additional structural traits are relevant. Species-specific architectural characteristics—including leaf distribution, branching pattern, and self-shading—likely influence projected silhouette coverage [24].

Because the octant method captures a defined vertical window (80–200 cm), observed changes partly reflect dynamic regeneration processes, with individuals growing into and out of the browsing-relevant layer over time [22]. Increased variability within height classes is consistent with progressive stand densification and intensified competition. In beech-dominated regeneration, intraspecific competition promotes hierarchical differentiation [25], while in mixed stands, fast-growing light-demanding species intensify competitive interactions [24]. These processes generate structural heterogeneity even within similar height classes.

Climatic variability and browsing pressure provide additional ecological context. Drought influences regeneration through interactions among soil water availability, radiation, and site productivity [26,27], potentially altering recruitment success and structural heterogeneity [14,28]. The drought periods between 2019 and 2022 may therefore have contributed to the increased variability observed in structural metrics.

Browsing represents another potential driver of structural differentiation. Reviews across temperate forest ecosystems demonstrate that ungulate density and browsing pressure can negatively affect regeneration success and structural attributes when intensity exceeds species-specific tolerance thresholds [1,2,5]. Browsing effects are species-specific and may interact with light and resource availability, influencing three-dimensional vegetation structure [29–31]. This interaction between browsing and light availability has recently been demonstrated experimentally, showing that regeneration outcomes depend on the combined influence of radiation conditions and herbivore pressure [32] (Lettenmaier et al., 2025). Such mechanisms may contribute to interspecific differences in structural patterns even where overall hunting regime effects remain weak. Interactions between climatic stress and herbivory are increasingly recognized, and cumulative drought conditions may interact with browsing to shape regeneration dynamics. While not directly tested here, these pathways provide ecological context for the heterogeneous patterns observed.

Structural metrics such as visual obstruction coverage and fractal complexity may also relate to habitat characteristics relevant for browsing ungulates. Vegetation density influences concealment and flight behaviour, and reduced flight distances have been documented in dense habitats [21]. However, behavioural or energetic consequences were not measured, and any linkage between obstruction and browsing frequency remains hypothetical.

Overall, visual obstruction coverage represents an integrative structural metric reflecting species morphology, competitive interactions, site conditions, climatic variability, and browsing within a dynamic successional context rather than a single causal driver.

4.2. Box Dimension Results

Differences in LiDAR-derived structural complexity (box-dimension, $D_{(b)}$) among federal states are consistent with variation in site-specific growth conditions and regeneration productivity. Structural complexity derived from mobile handheld laser scanning reflects the occupation of three-dimensional space and integrates density, layering, and spatial arrangement [33]. Fractal-based LiDAR studies demonstrate that $D_{(b)}$ captures emergent stand properties beyond single attributes such as basal area or mean height, instead reflecting spatial configuration [34,35]. Higher complexity values corresponded to regions characterized by greater site productivity, supporting the interpretation that environmental gradients and successional development represent primary drivers of structural differentiation.

Differences between fenced and unfenced plots suggest that ungulate exclusion may influence structural development, although the magnitude and direction of this effect were context dependent. Understory complexity results from interacting drivers including light availability, competition, and vegetation composition rather than a single factor [36]. Increased light availability following canopy reduction can alter competitive dynamics and vegetation structure [22,37], while also interacting with drought-related processes [26]. Consequently, ungulate exclusion does not necessarily result in uniform increases in $D_{(b)}$.

Species-specific differences in box-dimension are consistent with $D_{(b)}$ as an architectural metric, as branching patterns and growth strategies determine spatial biomass distribution [33]. The broadly similar increases in complexity between 2019 and 2023 across regions and species indicate that successional development and biomass accumulation acted as common drivers during the study period, consistent with structural accrual across developmental stages [34].

Any potential browsing-related effects were small relative to regional and temporal variation and remained below the detection threshold of the applied structural metrics. Browsing can reduce biomass but may also increase heterogeneity through gap formation and altered competitive hierarchies [30]. These opposing mechanisms may offset each

other within an integrated metric such as box-dimension, resulting in limited net effects. This interpretation is consistent with recent conceptual syntheses describing browsing effects as non-linear, context-dependent processes mediated by thresholds in regeneration tolerance, competitive release, and feedbacks between vegetation structure and herbivore behavior [36].

The divergence between visual obstruction coverage and $D_{(b)}$ underscores that both metrics quantify distinct structural dimensions. Visual obstruction represents an individual-based, perspective-oriented measure of concealment, whereas box-dimension summarizes plot-level space filling and structural heterogeneity derived from the point cloud [35]. The observed negative association between plant density (proxied by distance to plot center) and structural complexity aligns with the expectation that denser regeneration occupies three-dimensional space more extensively.

4.3. Limitations of the Study

Despite the integrative approach combining field-based visual obstruction measurements with LiDAR-derived structural complexity, several limitations must be considered. The classification of hunting regimes was based on information provided by hunting-right holders. Although cross-validated using field data, causal inferences regarding management effects remain limited, as observational designs inherently constrain attribution of structural patterns to individual drivers [7]. This limitation aligns with recent syntheses emphasizing the context dependency of browsing impacts across European forest ecosystems [36].

The study period from 2019 to 2023 represents a relatively short interval relative to forest developmental processes. Structural responses to browsing or management interventions may emerge only after temporal delays [37,38].

Structural metrics such as visual obstruction coverage and box-dimension describe architectural properties but do not capture demographic processes such as survival, recruitment, or individual browsing intensity. Remote sensing approaches primarily quantify geometric structure rather than physiological or demographic processes [39], and mechanistic links between ungulate activity and structural change therefore remain indirect.

Regional heterogeneity in site conditions and species composition introduces variability that may mask subtle management effects. Structural complexity is strongly shaped by environmental gradients and productivity differences [40], complicating the isolation of hunting-related signals.

Furthermore, LiDAR-based complexity metrics capture structural elements irrespective of biological origin. Deadwood components and vertical irregularities contribute to calculated complexity without distinguishing between living and dead biomass. While deadwood is a key structural habitat component [41], $D_{(b)}$ therefore reflects spatial configuration rather than species diversity or functional composition.

At the same time, this represents a methodological strength. LiDAR enables holistic quantification of three-dimensional habitat structure and has become well established for characterizing vertical layering, canopy density, and structural heterogeneity relevant for wildlife [4,42,43]. Recent TLS-based studies demonstrate that stem density and three-dimensional structure influence viewshed properties and landscape perception in deer [9,44]. However, LiDAR primarily provides geometric information and allows limited inference regarding species identity or trophic interactions [45]. Interpretation of structural complexity as habitat quality therefore requires ecological contextualization.

The combination of field-based and remote sensing approaches integrates complementary structural perspectives but does not replace demographic or population-based analyses necessary to establish causal relationships. Terrestrial laser scanning has rapidly advanced

as a core tool in forest ecology, enabling increasingly detailed and scalable quantification of three-dimensional forest structure and ecosystem processes [46]. Continued methodological development and integration with ecological and behavioural data will further enhance its potential for understanding forest–ungulate interactions. Recent advances in wildlife monitoring further demonstrate the potential of integrating structural forest metrics with direct assessments of ungulate presence and activity. For example, drone-based thermal imaging has recently been applied to assess wildlife impacts on forest regeneration at high spatial resolution [47]. Such approaches may complement LiDAR-based structural analyses by linking habitat structure more directly to animal distribution and behaviour, thereby strengthening causal inference in future studies.

5. Conclusions

This study demonstrates that handheld LiDAR is a robust tool for quantifying three-dimensional forest structure within the ungulate browsing zone and for disentangling the relative roles of succession, site conditions, and ungulate influence. Structural complexity increased consistently across regions between 2019 and 2023, indicating that site productivity and successional dynamics were the dominant drivers of forest structure. In contrast, management-related effects were weak, inconsistent, and statistically non-significant, indicating that hunting regime, as implemented and classified here, did not generate a consistent structural signal within the observation period, rather than producing uniform structural signals [40].

While LiDAR-derived complexity was largely insensitive to management treatments, visual obstruction captured habitat attributes behaviourally relevant to roe deer, consistent with findings linking structural density, concealment, and flight behaviour [48,49]. Moreover, stand structural complexity has been linked to management regimes and tree species diversity, with implications for microclimate regulation and ecosystem functioning [50]. The partial independence of complexity and visibility metrics aligns with recent advances distinguishing structural openness, visibility, and heterogeneity as separate ecological dimensions [51]. Integrating LiDAR-based metrics with targeted field indicators therefore strengthens structural monitoring and supports evidence-based forest and wildlife management. While site conditions and successional dynamics dominate three-dimensional complexity, integrating LiDAR metrics with behaviourally meaningful indicators improves the assessment of ungulate impacts and provides a stronger basis for evidence-based forest and wildlife management [52].

Author Contributions: Conceptualization, C.C.J.-F.; methodology, C.C.J.-F.; software, D.S., K.G. and C.C.J.-F.; validation, C.C.J.-F. and K.G.; formal analysis, C.C.J.-F. and K.G.; investigation, C.C.J.-F. and K.G.; resources, C.C.J.-F. and M.G.M.; data curation, C.C.J.-F. and K.G.; writing—original draft preparation, C.C.J.-F., K.G. and D.S.; writing—review and editing, D.S., M.G.M. and C.C.J.-F.; visualization, C.C.J.-F. and K.G.; supervision, D.S., M.G.M. and C.C.J.-F.; project administration, C.C.J.-F. and M.G.M. All authors have read and agreed to the published version of the manuscript.

Funding: This research received no external funding.

Data Availability Statement: The datasets presented in this article are not readily available because the data are part of an ongoing study. Requests to information about the datasets should be directed to claudia.jordan-fragstein@tu.dresden.de.

Acknowledgments: We would like to thank Robert Schlicht (TU Dresden) for statistical support.

Conflicts of Interest: The authors declare no conflicts of interest.

Abbreviations

The following abbreviations are used in this manuscript:

ANOVA	Analysis of Variance
APA	American Psychological Association
BB	Brandenburg
BW	Baden-Württemberg
$D_{(b)}$	Box dimension (measure of structural complexity)
GPS	Global Positioning System
LiDAR	Light Detection and Ranging
MV	Mecklenburg–Western Pomerania
NRW	North Rhine–Westphalia
RP	Rhineland-Palatinate
SL	Saarland
SN	Saxony
ST	Saxony-Anhalt
TH	Thuringia
TLS	Terrestrial Laser Scanning

References

1. Côté, S.D.; Rooney, T.P.; Tremblay, J.-P.; Dussault, C.; Waller, D.M. Ecological impacts of deer overabundance. *Annu. Rev. Ecol. Evol. Syst.* **2004**, *35*, 113–147. [CrossRef]
2. Ramirez, J.I.; Jansen, P.A.; Poorter, L.; den Ouden, J. Effects of wild ungulates on regeneration, structure and functioning of temperate forests: A semi-quantitative review. *For. Ecol. Manag.* **2018**, *424*, 406–419. [CrossRef]
3. Maeda, E.E.; Brede, B.; Calders, K.; Disney, M.; Herold, M.; Lines, E.R.; Nunes, M.H.; Raumonen, P.; Rautiainen, M.; Saarinen, N.; et al. Expanding Forest Research with Terrestrial LiDAR Technology. *Nat. Commun.* **2025**, *16*, 8853. [CrossRef]
4. Ewald, M.; Dupke, C.; Heurich, M.; Müller, J.; Reineking, B. LiDAR remote sensing of forest structure and GPS telemetry data provide insights on winter habitat selection of European roe deer. *Forests* **2014**, *5*, 1374–1390. [CrossRef]
5. Gill, R.M.A. A review of damage by mammals in north temperate forests: 3. Impact on trees and forests. *For. Int. J. For. Res.* **1992**, *65*, 363–388. [CrossRef]
6. Rooney, T.P.; Waller, D.M. Direct and indirect effects of white-tailed deer in forest ecosystems. *For. Ecol. Manag.* **2003**, *181*, 165–176. [CrossRef]
7. Didion, M.; Kupferschmid, A.D.; Bugmann, H. Long-term effects of ungulate browsing on forest composition and structure. *For. Ecol. Manag.* **2009**, *258*, 44–55. [CrossRef]
8. Bässler, C.; Stadler, J.; Müller, J.; Förster, B.; Göttlein, A.; Brandl, R. LiDAR as a rapid tool to predict forest habitat types in Natura 2000 networks. *Biodivers. Conserv.* **2011**, *20*, 465–481. [CrossRef]
9. Batchelor, J.L.; Wilson, T.M.; Olsen, M.J.; Ripple, W.J. New structural complexity metrics for forests from single terrestrial lidar scans. *Remote Sens.* **2022**, *14*, 145. [CrossRef]
10. Kolo, H.; Hilmers, T.; Ammer, C. Predicting natural regeneration in temperate forests based on site and stand variables. *For. Ecol. Manag.* **2017**, *404*, 202–214. [CrossRef]
11. Hofmann, R.R.; Streich, W.J.; Fickel, J.; Hummel, J.; Clauss, M. Convergent evolution in feeding types: Salivary gland mass differences in wild ruminant species. *J. Morphol.* **2008**, *269*, 240–257. [CrossRef]
12. Reimoser, F.; Suchant, R. Systematische Kontrollzäune zur Feststellung des Wildeinflusses auf die Waldvegetation. *Allgemeine Forst- und Jagdzeitung* **1992**, *163*, 27–31.
13. Tufto, J.; Andersen, R.; Linnell, J.D.C. Habitat use and ecological correlates of home range size in a small cervid: The roe deer. *J. Anim. Ecol.* **1996**, *65*, 715–724. [CrossRef]
14. Lovari, S.; San José, C. Woodlands and stone martens: Habitat use and density estimates in relation to habitat structure. *J. Zool.* **1997**, *242*, 91–100. [CrossRef]
15. Coulon, A.; Morellet, N.; Goulard, M.; Cargnelutti, B.; Angibault, J.-M.; Hewison, A.J.M. Inferring the effects of landscape structure on roe deer (*Capreolus capreolus*) movements using a step selection function. *Landsc. Ecol.* **2008**, *23*, 603–614. [CrossRef]
16. Saïd, S.; Gaillard, J.-M.; Widmer, O.; Débias, F.; Bourgoin, G.; Delorme, D.; Roux, C. What shapes intra-specific variation in home range size? A case study of female roe deer (*Capreolus capreolus*). *Oikos* **2009**, *118*, 1299–1306. [CrossRef]
17. Lanz, J.D.; Arnold, W.; Hackländer, K.; Ruf, T. Structural habitat components rather than food availability determine habitat use of European roe deer (*Capreolus capreolus*) in winter. *Eur. J. Wildl. Res.* **2018**, *64*, 38.

18. von der Goltz, H.; Ammer, C.; Vor, T.; Müller, M.; Jordan-Fragstein, C.; Knoke, T.; Bödeker, K.; Zimmer, R. BioWild—Biodiversity and Ungulate Management in Managed Forests: Final Report. ANW Deutschland e. V. 2022. Available online: https://www.biowildprojekt.de/media/biowild_schlussbericht_endf_3.pdf (accessed on 11 February 2026). (In German)
19. Andersen, R.; Duncan, P.; Linnell, J.D.C. *The European Roe Deer: The Biology of Success*; Scandinavian University Press: Oslo, Norway, 1998.
20. Vospernik, S.; Reimoser, S. Modelling changes in roe deer habitat in response to forest management. *For. Ecol. Manag.* **2008**, *255*, 530–545. [CrossRef]
21. Seidel, D. A holistic approach to determine tree structural complexity based on laser scanning data and fractal analysis. *Ecol. Evol.* **2018**, *8*, 128–134. [CrossRef]
22. Bartsch, N.; Röhrig, E. *Waldökologie: Einführung Für Mitteleuropa*, 4th ed.; Springer Spektrum: Berlin, Germany, 2016.
23. Ellenberg, H.; Weber, H.E.; Düll, R.; Wirth, V.; Werner, W.; Paulissen, D. *Zeigerwerte von Pflanzen in Mitteleuropa*; Scripta Geobotanica 18; Goltze: Göttingen, Germany, 2001.
24. Wagner, S. *Waldverjüngung und Jungwuchspflege*; UTB: Stuttgart, Germany, 2021.
25. Bartsch, N.; Ammer, C. Konkurrenz und Stabilität von Waldbeständen. In *Waldökologie*; Bartsch, N., Ed.; Springer: Berlin, Germany, 2010; pp. 243–280.
26. Larcher, W. *Physiological Plant Ecology*, 4th ed.; Springer: Berlin, Germany, 2001.
27. Blume, H.-P. *Handbuch des Bodens*; Springer Spektrum: Heidelberg, Germany, 2010.
28. Schulze, E.-D.; Beck, E.; Müller-Hohenstein, K. *Pflanzenökologie*; Spektrum Akademischer Verlag: Heidelberg, Germany, 2002.
29. Senn, J.; Häusler, J. Influence of ungulate browsing on forest regeneration. *Swiss For. J.* **2005**, *156*, 343–350.
30. Osterloher, P.; Wiechmann, H. Reaktionen junger Waldbäume auf Verbiss. *Forstarchiv* **1993**, *64*, 73–79.
31. Danell, K.; Huss-Danell, K.; Bergström, R. Interactions between browsing and plant growth. *Oikos* **1994**, *70*, 259–266. [CrossRef]
32. Lettenmaier, L.; Mysterud, A.; Mitesser, O.; Ammer, C.; Hothorn, T.; Cesarz, S.; Pierick, K. Light and ungulate browsing interact in shaping future woody plant diversity through natural regeneration. *J. Appl. Ecol.* **2025**, *62*, 3367–3380. [CrossRef]
33. Seidel, D.; Ehbrecht, M.; Annighöfer, P.; Ammer, C. From tree to stand-level structural complexity—Which properties make a forest stand complex in structure? *Agric. For. Meteorol.* **2019**, *278*, 107699. [CrossRef]
34. Seidel, D.; Ehbrecht, M.; Annighöfer, P.; Ammer, C. Deriving stand structural complexity from airborne laser scanning data—What does it tell us about a forest? *Remote Sens.* **2020**, *12*, 1854. [CrossRef]
35. Hardalau, D.; Codrean, C.; Iordache, D.; Fedorca, M.; Ionescu, O. The Expanding Thread of Ungulate Browsing—A Review of Forest Ecosystem Effects and Management Approaches in Europe. *Forests* **2024**, *15*, 1311. [CrossRef]
36. Seidel, D.; Ehbrecht, M.; Puettmann, K.; Annighöfer, P. From tree to stand level: Assessing forest structural complexity with terrestrial laser scanning. *For. Ecol. Manag.* **2017**, *394*, 53–63. [CrossRef]
37. Seidel, D.; Annighöfer, P.; Ammer, C.; Ehbrecht, M.; Willim, K.; Bannister, J.; Soto, D.P. Quantifying understory complexity in unmanaged forests using TLS and identifying some of its major drivers. *Remote Sens.* **2021**, *13*, 1513. [CrossRef]
38. Lefsky, M.A.; Cohen, W.B.; Parker, G.G.; Harding, D.J. Lidar remote sensing for ecosystem studies. *BioScience* **2002**, *52*, 19–30. [CrossRef]
39. Ehbrecht, M.; Seidel, D.; Annighöfer, P.; Kreft, H.; Köhler, M.; Zemp, D.C.; Puettmann, K.; Nilus, R.; Babweteera, F. Global patterns and climatic controls of forest structural complexity. *Nat. Commun.* **2017**, *8*, 1167. [CrossRef] [PubMed]
40. Müller, J.; Bütler, R. A review of habitat thresholds for dead wood: A baseline for management recommendations in European forests. *Eur. J. For. Res.* **2010**, *129*, 981–992. [CrossRef]
41. Vierling, K.T.; Vierling, L.A.; Gould, W.A.; Martinuzzi, S.; Clawges, R.M. Lidar: Shedding new light on habitat characterization and modeling. *Front. Ecol. Environ.* **2008**, *6*, 90–98. [CrossRef]
42. Davies, A.B.; Asner, G.P. Advances in animal ecology from 3D-LiDAR ecosystem mapping. *Trends Ecol. Evol.* **2014**, *29*, 681–691. [CrossRef] [PubMed]
43. Gresham, A.; Healey, J.R.; Eichhorn, M.P.; Barton, O.; Smith, A.R.; Shannon, G. Horizontal viewsheds of large herbivores as a function of woodland structure. *Ecol. Evol.* **2023**, *13*, e10699. [CrossRef] [PubMed]
44. Zellweger, F.; De Frenne, P.; Lenoir, J.; Rocchini, D.; Coomes, D.A. Advances in microclimate ecology arising from remote sensing. *Trends Ecol. Evol.* **2019**, *34*, 327–341. [CrossRef]
45. Boardman, N.K. Comparative photosynthesis of sun and shade plants. *Annu. Rev. Plant Physiol.* **1977**, *28*, 355–377. [CrossRef]
46. Calders, K.; Adams, J.; Armston, J.; Bartholomeus, H.; Bauwens, S.; Bentley, L.P.; Chave, J.; Danson, F.M.; Demol, M.; Disney, M.; et al. Terrestrial laser scanning in forest ecology: Expanding the horizon. *Remote Sens. Environ.* **2020**, *251*, 112102. [CrossRef]
47. Jordan-Fragstein, C.C.; Müller, M.G.; Bielefeld, N.; Georgi, R.; Friedrich, R. Assessing wildlife impact on forest regeneration through drone-based thermal imaging. *Forests* **2025**, *16*, 1787. [CrossRef]
48. Basnet, P. Deriving Forest Structural and Functional Metrics from LiDAR: A Multisource Analysis of Height, Species Diversity, and Soil Properties. Doctoral Dissertation, University of Göttingen, City of Göttingen, Germany, 2025. Available online: https://ediss.uni-goettingen.de/ (accessed on 15 January 2025).

49. Neumann, W.; Martinuzzi, S.; Estes, A.B.; Pidgeon, A.M.; Dettki, H.; Ericsson, G.; Radeloff, V.C. Opportunities for the application of advanced remotely-sensed data in wildlife habitat modeling. *Mov. Ecol.* **2015**, *3*, 6. [CrossRef]
50. Ehbrecht, M.; Schall, P.; Ammer, C.; Seidel, D. Quantifying stand structural complexity and its relationship with forest management, tree species diversity and microclimate. *Agric. For. Meteorol.* **2017**, *242*, 1–9. [CrossRef]
51. Fattorini, N.; Brunetti, C.; Baruzzi, C.; Lovari, S. Temporal variation in vigilance behaviour of roe deer (*Capreolus capreolus*) in relation to habitat structure and human disturbance. *Behav. Process.* **2020**, *172*, 104044.
52. Ionescu, O.; Hardalau, D.; Bakševičius, M.; Manton, M.; Popovici, D.C.; Codrean, C.; Iordache, D. Tracking population trends: Insights from deer hunting harvests in the Baltics, Central, and Eastern Europe. *Cent. Eur. For. J.* **2025**, *71*, 83–96. [CrossRef]

Disclaimer/Publisher's Note: The statements, opinions and data contained in all publications are solely those of the individual author(s) and contributor(s) and not of MDPI and/or the editor(s). MDPI and/or the editor(s) disclaim responsibility for any injury to people or property resulting from any ideas, methods, instructions or products referred to in the content.